Cerebral Cortex June 2010;20:1274–1285
doi:10.1093/cercor/bhp194
Advance Access publication September 24, 2009

Neural Modulation of Temporal Encoding, Maintenance, and Decision Processes

Deborah L. Harrington[1,2], Janice L. Zimbelman[3], Sean C. Hinton[4,5] and Stephen M. Rao[3,4]

[1]Department of Radiology, University of California, San Diego, CA 92093, USA, [2]VA San Diego Healthcare System, San Diego, CA 92161, USA, [3]Neurological Institute, Cleveland Clinic, Cleveland, OH 44195, USA, [4]Department of Neurology, Medical College of Wisconsin, Milwaukee, WI 53226, USA and [5]Abbott Laboratories, Abbott Park, IL 60064, USA

Time perception emerges from an interaction among multiple processes that are normally intertwined. Therefore, a challenge has been to disentangle timekeeping from other processes. Though the striatum has been implicated in interval timing, it also modulates nontemporal processes such as working memory. To distinguish these processes, we separated neural activation associated with encoding, working-memory maintenance, and decision phases of a time-perception task. We also asked whether neuronal processing of duration (i.e., pure tone) was distinct from the processing of identity (i.e., pitch perception) or sensorimotor features (i.e., control task). Striatal activation was greater when encoding the duration than the pitch or basic sensory features, which did not differentially engage the striatum. During the maintenance phase, striatal activation was similar for duration and pitch but at baseline in the control task. In the decision phase, a stepwise reduction in striatal activation was found across the 3 tasks, with activation greatest in the timing task and weakest in the control task. Task-related striatal activations in different cognitive phases were distinguished from those of the supplementary motor area, inferior frontal gyrus, thalamus, frontoparietal cortices, and the cerebellum. Our results were consistent with a model in which timing emerges from context-dependent corticostriatal interactions.

Keywords: cerebral cortex, cognition, fMRI, striatum, timing, working memory

Introduction

Interval timing is fundamental to many aspects of behavior, yet despite decades of research, its neural substrate remains debated due to the difficulty in disentangling its different component processes. For example, one dominant model (Meck 1983, 1996) posits an internal clock consisting of a dopamine-regulated pacemaker that generates pulses and an accumulator that counts pulses during a time period, thereby representing perceived duration. The experience of time, however, can be dilated or compressed by working memory (WM) and decisional processes (Gibbon et al. 1984).

In a functional magnetic resonance imaging (fMRI) study, we identified the neural correlates of encoding and decisional processes associated with interval timing (Rao et al. 2001) by having participants judge whether a comparison interval (CI) was longer or shorter than a standard interval (SI); the intervals were separated by a 1-s delay. Encoding the SI produced activation of the basal ganglia and right inferior-parietal cortex, whereas decision making during the CI activated the cerebellum and right dorsolateral prefrontal cortex (PFC). In a subsequent study, with SI and CI separated by slightly longer delays (2.2–2.8 s), timing proficiency correlated with right caudate and parietal cortex activation during encoding, whereas time-discrimination difficulty correlated with a WM network during decision making (Harrington et al. 2004).

Although our results were consistent with models that implicate the striatum and dopamine neurotransmission in interval timing (Meck 1996), the striatum is also engaged by WM (Postle and D'Esposito 1999). Thus, striatal activation during the encoding and/or the decision phases could be due to maintaining the interval representation in WM. Due to the short delays between the SI and CI, our studies and others (Coull et al. 2008) could not distinguish neural systems involved in the maintenance of temporal information. In the present study, we extended the delay to 10 and 12.5 s, thereby also permitting a better separation of neural systems mediating interval encoding and decision making.

We also asked whether neuronal processing of duration, demarcated by auditory stimuli, was distinct from the processing of identity features (i.e., pitch). Recent WM (Hazy et al. 2006) and temporal processing (Matell and Meck 2004) models emphasize, respectively, the representation of identity and duration information and share the concept of coincidence detection of cortical oscillation patterns by medium spiny neurons in the striatum. In the computational model (Hazy et al. 2006), PFC encodes and passively maintains information in WM and the striatum actively maintains WM by updating PFC. In the striatal beat frequency (SBF) model (Matell and Meck 2004), timing emerges from activation of striatal neurons by the onset and offset of synchronized cortical oscillators that define an event. Striatal neurons detect and trigger responses to identity information encoded by cortical neurons and temporal information encoded by their oscillatory state over time (Lustig et al. 2005). The variability of individual oscillators is thought to become increasingly noisy over time (Matell and Meck 2004), which accounts for increases in timing variability that are proportional to the interval duration. However, perception of identity tends to be rapid and automatic. Though not specifically addressed by the model, this may suggest that striatal detection of cortical patterns defining stimulus identity is more automatic when duration is irrelevant. We, therefore, hypothesized that striatal activation would be greater when encoding duration than pitch, as the former requires continuous integration of cortical oscillatory states during a stimulus and presumably more striatal resources. In contrast, we predicted that striatal activation for duration and pitch would be similar when maintaining information in WM.

Materials and Methods

Participants

Twenty healthy adults participated in this study (13 female; mean age = 29 years, range: 19 to 48 years, standard deviation [SD] = 9.1; mean

education = 15 years, range: 12–18 years, SD = 1.5). Participants were excluded if they had a history of neurologic disturbance (e.g., seizures, head injury), learning disability or mental retardation, major psychiatric disturbance, or substance abuse. All participants were strongly right handed, as determined by the Edinburgh Handedness Inventory (Oldfield 1971) and gave their written informed consent according to guidelines of the Institutional Review Board of the Medical College of Wisconsin, Milwaukee.

fMRI Tasks

Participants performed 3 tasks in the scanner: time discrimination (T), pitch discrimination (P), and sensorimotor control (C), the order of which was counterbalanced across subjects. Each task consisted of the sequential presentation of 4 16-bit sine waves sampled at 44.1 kHz (Fig. 1*a*). The tone stimuli, each 50 ms in duration, were amplified near the scanner and delivered to the participant via air conduction through 180-cm paired plastic tubes, which were threaded through occlusive ear inserts that attenuated background scanner noise to a sound pressure level of approximately 75 dB. For each trial, participants made a 2-choice key-press response using the index or middle finger of their right (dominant) hand using a custom-made piano-style keyboard device.

In the T task, participants indicated whether the time interval between tones 3 and 4 (CI) was shorter (index finger) or longer (middle finger) than the time interval between tones 1 and 2 (SI). Three SIs (1090, 1200, and 1321 ms) were employed to increase the demands of maintaining an interval across the delay period. For each SI, participants were presented with 1 of 3 CI (3 shorter, 3 longer). The CI were approximately 9.2%, 17.5%, and 25% shorter or longer than the SI. For example, the SI of 1090 ms had CI of 817, 899, 990, 1200, 1321, and 1454 ms. The CI used for each SI are displayed in Figure 1*b*. All 4 tones were of the same pitch (700 Hz).

In the P task, participants indicated whether tones 3 and 4 (comparison frequency) were lower (index finger) or higher (middle finger) in pitch than the first pair of tones (standard frequency). This procedure differed from our previous study (Rao et al. 2001), in which the pitch of the first 3 tones (standard) was the same and the pitch of the fourth tone (comparison) differed. A limitation of this design was that the first 2 tones may not have been encoded because pitch discriminations could be carried out by comparing the third (standard) and the fourth tone (comparison). In the current study, this was not possible, because the first 2 tones were the standard and the last 2 tones were the comparison. As displayed in Figure 1*c*, tones 1 and 2 consisted of 1 of 3 standard frequencies (695.30, 700.00, and 704.73 Hz). For each standard frequency, participants were presented with 3 comparison frequencies (3 lower, 3 higher). The comparison frequencies were approximately 0.92%, 1.35%, and 2% lower or higher than the standard frequency. For example, the standard frequency 695.3 Hz had comparison frequencies of 681.4, 686.0, 690.6, 700.0, 704.7, and 709.5 Hz.

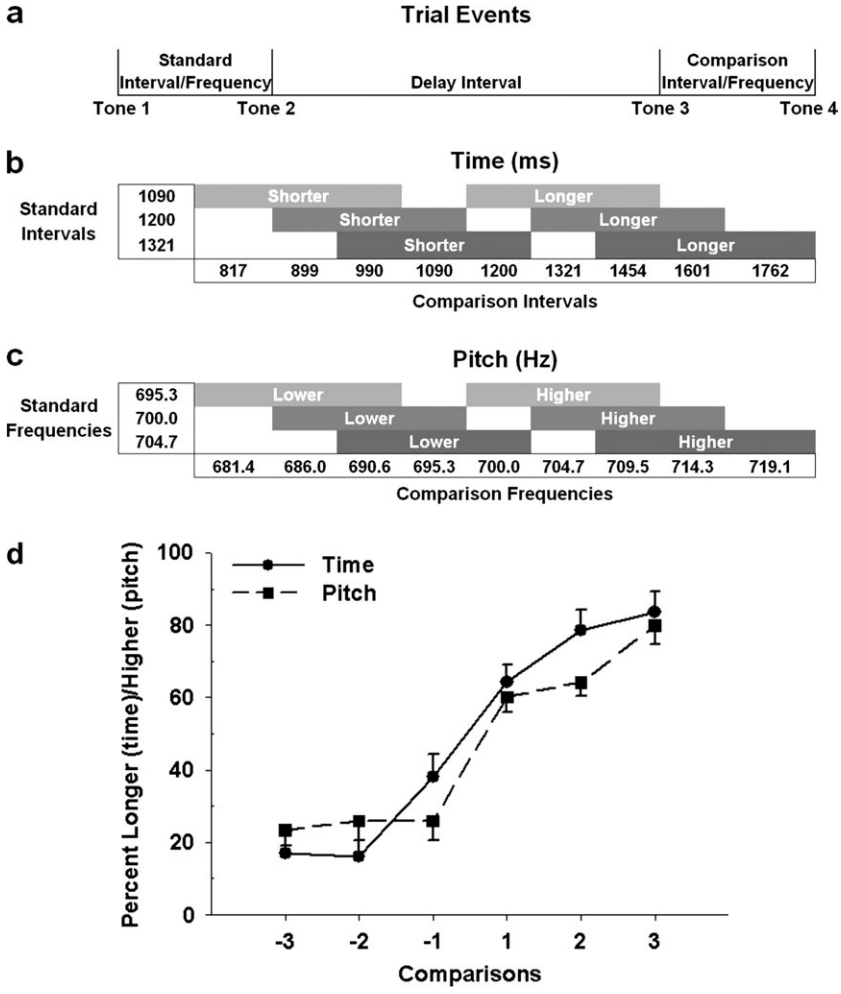

Figure 1. Time and pitch discrimination task designs and performance. (*a*) Trial events, (*b*) Standard and comparison intervals for the time-discrimination task, (*c*) Standard and comparison frequencies for the pitch discrimination task, (*d*) Accuracy data from the time and pitch discrimination tasks, averaged across the 2 delay periods. Accuracy data were converted to the mean percent longer and percent higher for the time and pitch tasks, respectively. Data were averaged across the 3 SI/pitch tasks and their respective comparisons. For the time task, ± 1, 2, and 3 designate CIs that were approximately 9.2%, 17.5%, and 25% shorter (negative values) or longer (positive values) than the SI. For the pitch task, ±1, 2, and 3 designate comparison pitches that were approximately 0.92%, 1.35%, and 2% lower (negative values) or higher (positive values) than the standard pitch.

The comparison frequencies for each standard frequency are displayed in Figure 1*c*. The duration between tones 1 and 2 and between tones 3 and 4 was fixed at 1200 ms. For comparability, the SIs and pitches were within a similar range (1200 ms/700 Hz) as those used in our earlier study (Rao et al. 2001). Comparison intervals and pitches were chosen based on pilot testing that was conducted to ensure that the 2 tasks were of equivalent difficulty.

The C task controlled for the effects of low-level sensory and motor processing from the functional maps in the T and P discrimination tasks. The structure of stimulus events was similar to the T and P tasks. Two 700-Hz tones were presented at the onset of a trial; after a variable delay period, another 2 tones were presented. Each tone pair was separated by 1200 ms. Participants pressed a key with their right index finger after the presentation of the fourth tone.

Randomized delay periods of 10 and 12.5 s were employed for each task to separate neural systems supporting interval encoding and WM processes from those supporting decision making. Each task consisted of 36 trials, divided into 2 functional imaging runs of 18 trials each. The factors were 1) SI/standard frequency (3 levels), 2) delay period (2 levels), and 3) CI/comparison frequency (6 levels). Each possible combination of the 3 factors was presented once per task in a random order. Presentation order of the T, P, and C tasks was counterbalanced across subjects.

Image Acquisition

Event-related fMRI was performed using a 1.5-T scanner (Signa; GE Medical Systems, Milwaukee, WI) equipped with a 3-axis, local-gradient head coil and an elliptical, end-capped, quadrature radio-frequency coil. Foam padding limited head motion within the coil. Prior to functional imaging, high-resolution, 3D anatomic volumes were collected for anatomic localization and coregistration (time echo, TE 5 ms; time repetition, TR 24 ms; 40° flip angle; axial slice thickness = 1.2 mm; field of view [FOV] 24 cm; 256 × 192 matrix; and NEX = 1). Echo-planar images were collected using a single-shot, blipped, gradient-echo, echo-planar pulse sequence (TE 40 ms; TR 2500 ms; 90° flip angle; FOV 24 cm; 64 × 64 matrix; and number of excitations [NEX] = 1). Each functional imaging volume included 22 contiguous 6-mm sagittal slices to provide coverage of the entire brain. Presentation of the fixation point for each trial corresponded to the onset of a scanning volume. Each functional imaging run consisted of 200 volumes.

fMRI Data Analysis

Functional images were analyzed using Analysis of Functional Neuro-Images (AFNI; Cox 1996). Slice values were time shifted to the beginning of the TR for all slices using heptic interpolation. The first 5 and the last 2 volumes were removed from each run, and the runs were concatenated in the following order: Time1 (T1), T2, Pitch1 (P1), P2, Control1 (C1), and C2. The volumes were registered in 3 dimensions to the one collected closest to the acquisition of the anatomical images. The data for each participant were masked to exclude voxels having low signal intensity (using AFNI 3dAutomask with clfrac = 0.15), which generally fall either outside the brain or at the edges of the functional volumes. The time series data were blurred using a 6-mm full-width half-maximum Gaussian filter and then normalized to 1000 times the whole-brain average of the time series.

The time series for each participant was deconvolved using the trial onset for each task (T, P, and C) separated according to delay period (10.0 or 12.5 s). This analysis produces hemodynamic response functions (HRFs) of the fMRI signal on a voxelwise basis. The HRFs are estimates of the hemodynamic response for each condition relative to a baseline state and are generated without making a priori assumptions about the shape, delay, or magnitude of the HRF. The deconvolution was modeled for 8 or 9 time points for the 10.0 or 12.5-s delay period, respectively. HRFs were constrained to start from 0 by subtracting the value of the HRF at trial onset from each subsequent point. Area under the curve (AUC) was calculated for the different phases of each trial as follows: encoding corresponded to volumes 1–3 beginning at 2.5, 5.0, and 7.5 s, maintenance was identified as volumes 4 and 5 beginning at 10.0 and 12.5 s for the 10.0-s delay (or, for the 12.5-s delay period, volumes 4–6 beginning at 10.0, 12.5, and 15.0 s), and the decision phase was volumes 6–8 beginning at 15.0, 17.5, and 20.0 s for the 10.0-s delay (or, for the 12.5-s delay period, volumes 7–9 beginning at 17.5, 20.0, and 22.5 s). Figure 2 displays the time course of activation in representative regions for each task. This figure illustrates the images used in the 10-s delay condition to represent AUCs for the encode, maintenance, and decision phases.

Anatomical and functional volumes were individually interpolated to volumes with 1-mm^3 voxels, coregistered, and transformed to Talairach stereotaxic coordinate space (Talairach and Tournoux, 1988). Repeated-measures analyses of variance (ANOVAs) tests of the task main effect, with follow-up planned pairwise *t* tests (pooled variance), were performed on a voxelwise basis to generate statistical parametric maps that identified voxels showing greater activation in the T or the P tasks than in the C task and differing activation in the T versus the P task. We restricted comparisons with the C task to positive voxels (i.e., T > C, P > C). The T versus P comparison produced only clusters where T > P. Voxelwise thresholds were derived from 3000 Monte Carlo simulations using the AlphaSim procedure in AFNI, which computed the voxel probability and minimum cluster-size threshold needed to obtain a familywise alpha level of $P < 0.05$. Because the spatial threshold can bias the results against smaller activation clusters that were areas of interest (i.e., basal ganglia), statistical thresholds were derived

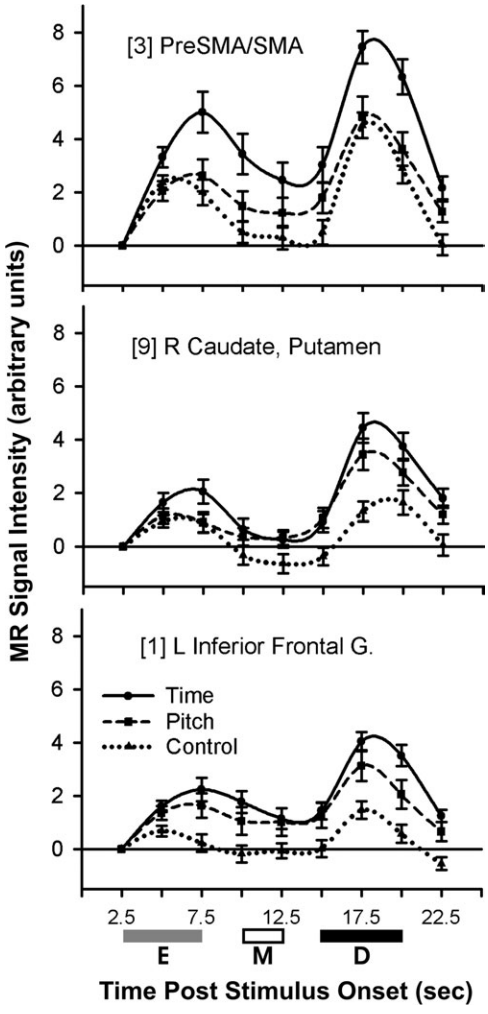

Figure 2. Time course of activation for the T, P, and C tasks in representative regions. Boxes along the *x*-axis indicate the time points selected in the short (10-s) delay condition to calculate the AUC for the encode (E: light gray), maintain (M: white) and decision (D: black) phases. Bracketed numbers refer to brain regions listed in Table 2 and displayed in Figure 4.

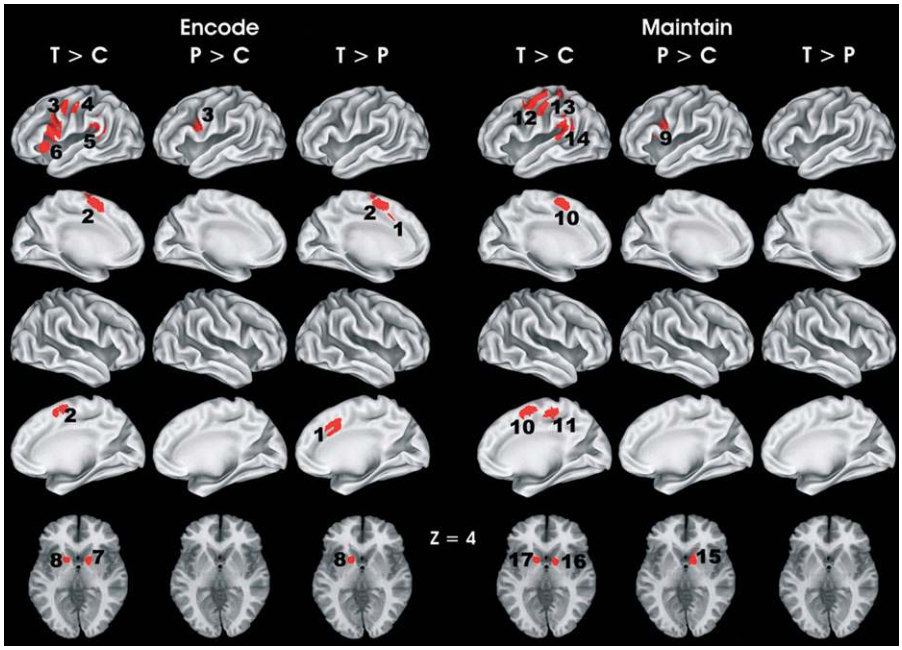

Figure 3. Results of the voxelwise ANOVA identifying regions showing significantly greater activation in the T or P tasks than the C task, or differing activation in the T versus the P task for the encode and maintenance phases. Numbers adjacent to activation foci correspond to numbers in Table 1.

separately for basal ganglia and cortical volumes (Worsley et al. 1996). This was accomplished by creating a basal ganglia mask that included the lentiform nucleus, claustrum, thalamus, and caudate structures identified from the Talairach Daemon data set (TTatlas + tlrc); the mask was then expanded to include any voxels within a 4-mm radius. The cortical mask included all other brain regions. Each mask was used in the Monte Carlo simulations to determine the appropriate combination of individual voxel probability and minimum cluster-size threshold. We used an individual voxel probability of $t = 3.55$ ($P < 0.001$, df = 38) with a minimum cluster size of 0.337 mL for cortical regions and $t = 2.98$ ($P < 0.005$, df = 38) with a minimum cluster size of 0.422 mL for the basal ganglia.

A functional region of interest (fROI) analysis was first performed to evaluate differences in the magnitude of the MR signal change estimates in activated regions. For each phase (encode, maintain, decision), an fROI map was generated by the activated regions identified in the voxelwise maps (Fig. 3) across the 3 comparisons (T > C, P > C, and T > P).

Because the regions of significant activation for the encode and the maintenance phases were similar (Fig. 3) and of central interest in our study, they were conjoined into one fROI map (Fig. 4) to directly test whether task-related patterns of activation differed between the 2 phases in the same ROI. In these analyses, repeated-measures ANOVAs tested the effects of task (T, P, and C), phase (encode, maintenance), and the interaction in each fROI. For fROI showing significant interactions or main effects of task, planned follow-up Fisher least significant difference tests were conducted to determine the locus of the task differences. Omnibus F tests were considered statistically significant at $\alpha = 0.01$ and planned comparisons at $\alpha = 0.05$. Results from these analyses were a focus of the discussion.

From the voxelwise maps that were generated for each of the 3 task comparisons during the decision–response phase (Fig. 6), we created a separate conjoined fROI map (Fig. 7) to directly compare differences in MR signal intensity across all 3 tasks. This map showed task-related activation in several additional regions that were not found during interval encoding or maintenance. Due to the large fROIs for the decision–response phase, we separated these into smaller fROIs along minimum contour lines of the T versus C voxelwise map using a watershed algorithm. This algorithm first uses AFNI 3dExtrema to find a set of local maxima separated by at least 20 mm and then creates boundaries for clusters containing these maxima along the minimum value contour lines (Cox 1996). One fROI did not separate well using a 20-mm separation distance, so 15 mm was used to separate that fROI.

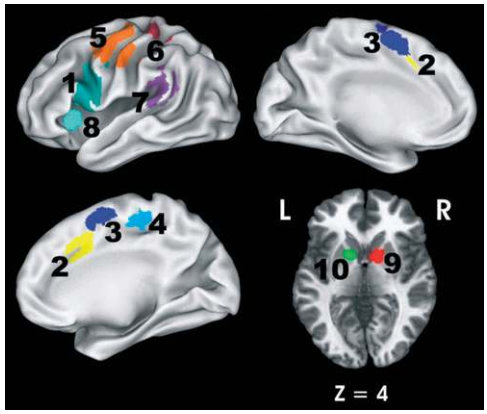

Figure 4. Functional ROIs of the encode/maintenance conjunction map used to evaluate differences in MR signal intensity across the T, P, and C tasks. Numbers adjacent to activation foci correspond to numbers in Table 2.

Results

Task Performance

In discrimination paradigms, accuracy is the dependent measure of interest. Accuracy was averaged across the 3 standard frequencies and 3 SIs as this variable was not a focus of the study. Per convention, the percent correct responses for each comparison interval and pitch were converted into percent "longer" (T task) and percent "higher" (P task) to generate discrimination functions that displayed the slope of the accuracy data (see Fig. 1*D*). This is a simple linear transformation, in which the percent correct responses for comparison stimuli that are shorter (T task) and lower (P task)

Table 1
Regions of activation from the separate voxelwise analysis of task effects for the encode and maintenance phases

	T > C				P > C				T > P			
	x	*y*	*z*	Vol.	*x*	*y*	*z*	Vol.	*x*	*y*	*z*	Vol.
Encode												
Frontal lobe												
[1] B anterior cingulate (6,8,32)									4	13	38	0.41
[2] B pre-SMA/SMA (6)	−5	2	54	1.77					−8	0	53	0.69
[3] L precentral, inferior frontal (6,9,44)	−48	5	20	2.60	−45	2	25	0.46				
Parietal lobe												
[4] L postcentral, Precentral (6)	−49	−9	43	0.64								
Temporal lobe												
[5] L superior temporal, insula (13)	−49	−39	18	0.66								
Limbic system												
[6] L insula (13)	−35	15	5	0.52								
Basal ganglia												
[7] R globus pallidus	14	4	3	0.80								
[8] L Putamen	−16	5	6	0.53					−15	6	5	0.54
Total activation volume				**7.52**				**0.46**				**1.64**
Maintenance												
Frontal lobe												
[9] L inferior frontal (44)					−41	6	23	0.39				
[10] B pre-SMA/SMA (6)	−1	1	54	1.25								
[11] R paracentral (6)	11	−23	51	0.57								
[12] L precentral (4,6)	−47	−11	46	1.93								
Parietal lobe												
[13] L Postcentral (3,4)	−33	−34	54	0.49								
Temporal lobe												
[14] L superior temporal, Inferior parietal (13)	−52	−39	19	1.39								
Basal ganglia												
[15] R caudate					11	6	3	1.17				
[16] R globus pallidus	12	3	4	0.59								
[17] L putamen	−14	9	−1	1.23								
Total activation volume				**7.45**				**1.56**				**0.00**

Note: Numbers on the left in brackets refer to brain regions displayed in Figure 3. Numbers in parentheses after the region label refer to Brodmann areas defined by the Talairach and Tournoux (1988) atlas. There were no significant regions of activation for the C > T, C > P, or P > T comparisons. Coordinates represent distance in mm from anterior commissure: *x*, right (+)/left (−); *y*, anterior (+)/posterior (−); *z*, superior (+)/inferior (−). Vol. = volume; L = left; R = right; and B = bilateral.

Table 2
Encode and maintenance phase functional ROIs and summary of statistical analyses

Region	*X*	*Y*	*Z*	Vol.	Task	Phase	Interaction	Encode phase			Maintenance phase		
					P	*P*	*P*	*P*	η^2	Contrast	*P*	η^2	Contrast
Frontal lobe													
[1] L inferior frontal gyrus (44,45)	−48	5	20	3.02	0.0001	0.02	ns	0.0001	0.46	T = P > C	0.001	0.30	T = P > C
[2] R anterior cingulate (32)	4	13	38	0.41	0.001	0.001	ns	0.001	0.35	T > P = C	0.05	0.18	T > P = C
[3] Pre-SMA/SMA(6)	−4	1	54	2.18	0.0001	0.0001	0.08*	0.0001	0.41	T > P = C	0.001.	0.32	T > P > C
[4] R paracentral lobule (6)	11	−23	51	0.57	0.002	ns	0.006	ns	0.13	—	0.0001	0.38	T > P > C
[5] L precentral gyrus (6)	−47	−10	46	2.07	0.0001	ns	ns	0.001	0.36	T > P = C	0.0001	0.47	T > P > C
Parietal lobe													
[6] L postcentral gyrus (3,40)	−33	−34	54	0.49	0.006	0.01	0.004	ns	0.09	—	0.001	0.33	T > P > C
Temporal lobe													
[7] L superior temporal gyrus (13)	−52	−39	18	1.64	0.0001	0.0001	ns	0.001	0.35	T > P = C	0.0001	0.45	T > P > C
Limbic system													
[8] L insula (13)	−35	15	5	0.52	0.0001	ns	0.03	0.0001	0.43	T > P = C	0.001	0.33	T = P > C
Basal ganglia													
[9] R caudate, putamen	12	6	3	1.62	0.002	0.01	0.007	0.01	0.22	T > P = C	0.001	0.33	T = P > C
[10] L caudate, putamen	−15	9	1	1.54	0.0001	0.02	0.06*	0.001	0.33	T > P = C	0.001	0.35	T = P > C

Note: Significance levels for the Omnibus F tests are reported under the Task, Phase, and Interaction columns. Asterisks designate regions showing a trend for a significant omnibus F test of the interaction, but a significant quadratic interaction component ($P = 0.004$ for pre-SMA/SMA; $P = 0.007$ for left caudate/putamen), indicating that task-related effects were nonlinear (i.e., T > P = C) in the encode but not the maintenance phase (i.e., T > P > C). ns = nonsignificant. Significance levels for separate main effect tests of task for each phase are reported in the Encode Phase and Maintenance Phase columns. Numbers in brackets on the left refer to brain regions displayed in Figure 4. Numbers in parentheses after the region label refer to Brodmann areas defined by the Talairach and Tournoux (1988) atlas. Coordinates represent distance in mm from anterior commissure: *x*, right (+)/left (−); *y*, anterior (+)/posterior (−); and *z*, superior (+)/inferior (−). *P* values are the result of the repeated-measures ANOVAs. Vol. = volume; L = left; and R = right.

are subtracted from 100%. To determine if the percent higher/longer responses were influenced by the delay period, separate repeated-measures ANOVAs were conducted for each task testing the effects of delay (10 and 12.5 s), comparison interval/pitch, and their interaction. The Huynh–Feldt correction was applied to all multiple df effects to adjust for violations of sphericity. For the T and P tasks, performance was not affected by the delay period, nor did it interact with comparison interval or pitch. As expected, there was a large effect of comparison interval ($F[2.4, 46] = 26.6$, $P < 0.0001$, $\eta^2 = 0.58$) and pitch ($F[3.2, 60] = 28.0$, $P < 0.0001$, $\eta^2 = 0.60$). Figure 1*d* plots the discrimination functions for each of the tasks, averaged across

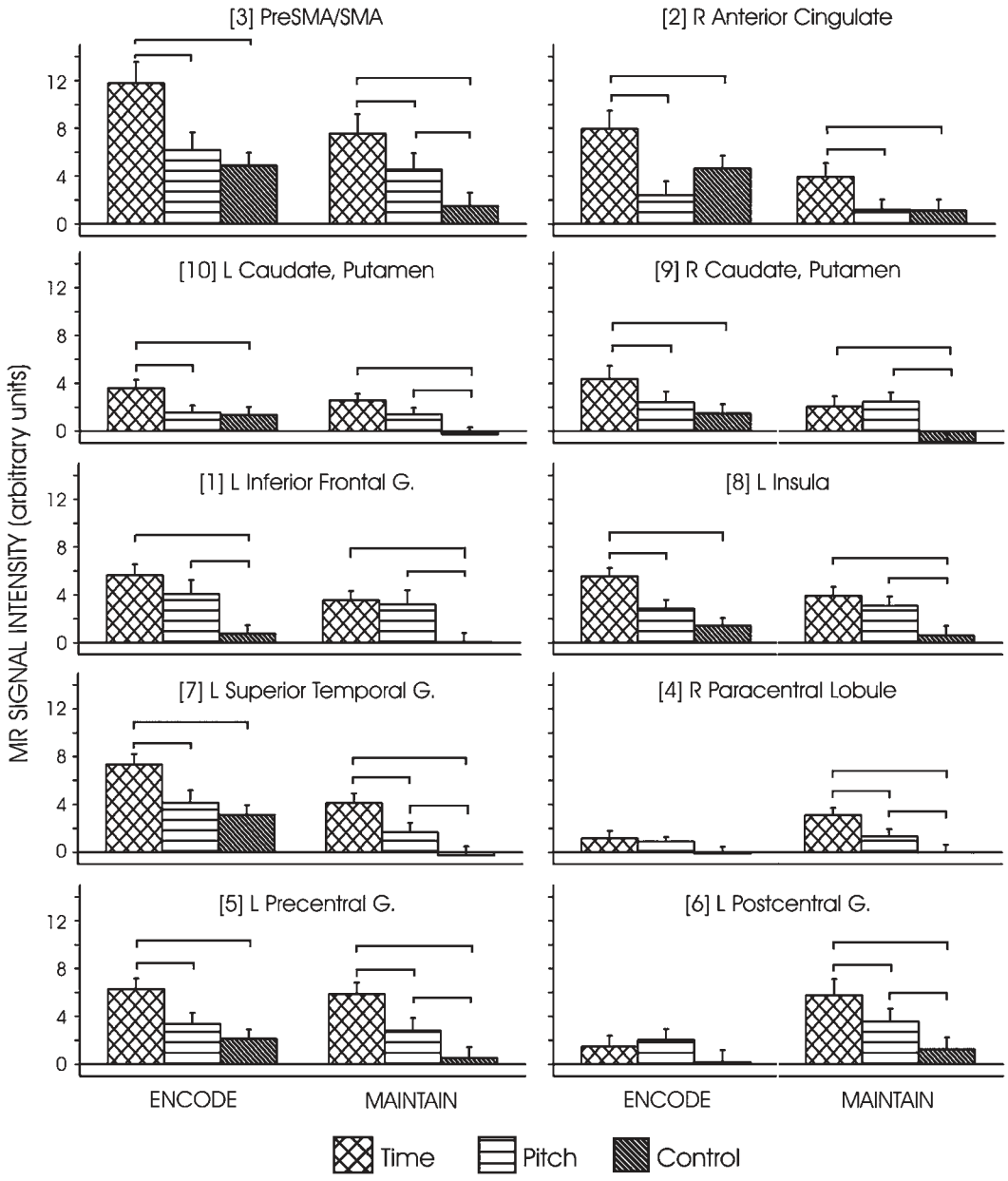

Figure 5. MR signal intensity for the T, P, and C tasks within each encode/maintenance conjunction map functional ROI. Bracketed numbers refer to brain regions listed in Table 2 and displayed in Figure 4; Horizontal lines indicate significant ($P < 0.05$) differences between conditions based on post hoc tests; error bars = standard error of the mean (SEM). L = left; R = right; and G = gyrus.

delay period. This figure suggests that accuracy in the 2 tasks was similar. This observation was confirmed by a repeated-measure ANOVA, in which the effect of task and the interaction of task × comparison interval/frequency were nonsignificant. This finding demonstrated that the T and P tasks were matched in difficulty.

fMRI Data

Encode and Maintenance Phases

Separate voxelwise analysis for the encode and maintenance phases demonstrated significant task-related activation in multiple cortical and subcortical regions (Fig. 3 and Table 1). For both phases, the spatial extent of activation was considerably greater for the T > C than the P > C comparison. For the encode phase, significant differences between the T and P tasks emerged in 3 regions: left putamen, bilateral supplementary motor area (SMA)/pre-SMA, and bilateral anterior cingulate. For the maintain phase, no differences were observed between the T and P tasks.

Next, differences in task-related MR signal intensity between the 2 phases were directly compared in 10 fROIs that were generated from a combined encode and maintenance conjunction map (Fig. 4) derived from the above voxelwise analyses (Fig. 3). For each fROI, MR signal intensity for the encode and the maintenance phases was calculated from the AUC of the averaged HRF for the T, P, and C tasks. These data were analyzed in a repeated-measures ANOVA that tested the effects of task (T, P, and C), phase (encode, maintenance), and the interaction (Table 2, Fig. 5).

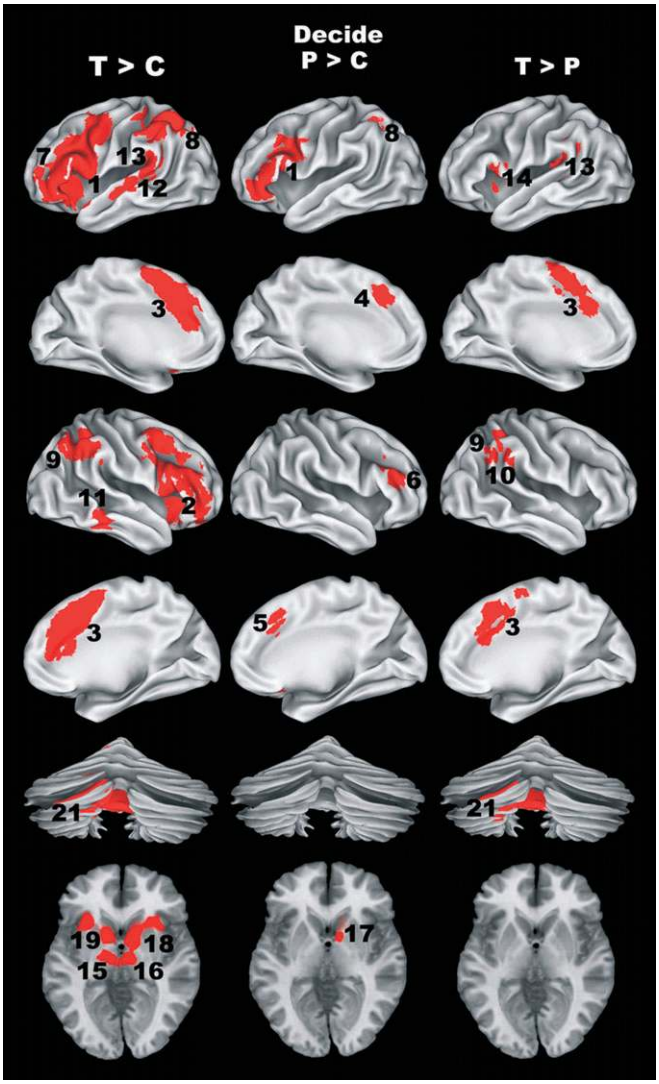

Figure 6. Results of the voxelwise ANOVA identifying regions of significantly greater activation in the T or P tasks than the C task, or differing activation in the T versus the P task for the decision phase. Numbers adjacent to activation foci correspond to numbers in Table 3.

Table 2 displays the results from repeated-measure ANOVA tests of the full model. All fROI showed a significant main effect of task. Most also exhibited a main effect of phase ($P = 0.01$) or a trend for an effect ($P = 0.02$), such that peak activation was greater in the encode than in the maintenance phase. Exceptions included the left postcentral gyrus, which exhibited greater activation in the maintenance than in the encode phase, and the left precentral gyrus, left insula, and right paracentral lobule, which did not show an effect of phase. These results were qualified by the significant task × phase interactions ($P = 0.01$) or trends for an interaction ($P = 0.03$) in the pre-SMA/SMA, right paracentral lobule, left postcentral gyrus, left insula, and bilateral caudate. Follow-up analyses verified that the interactions were due to different task-related patterns of activation between the 2 phases. During the encode phase (Table 2, left panels of Fig. 5), all of these regions showed greater activation for the T task than the P and C tasks (T > P = C), except the left postcentral gyrus and right paracentral lobule, which did not exhibit significant task-related activation. In contrast, 2 distinct task-related patterns of activation were found in these same regions during the maintenance phase (Table 2, right panels of Fig. 5). The pre-SMA/SMA, right paracentral lobule, and the left postcentral gyrus showed a stepwise activation function such that AUC was greatest for the T task and least for the C task (T > P > C). In the left insula and bilateral caudate, AUC in the T and P tasks was equivalent, but both were significantly greater than the C task (T = P > C).

Planned comparisons were also conducted for regions that did not show an interaction to delineate the patterns of task-related activation within each phase. For both the encode and the maintenance phases, activation in the left inferior frontal gyrus (IFG) was similar for the T and P tasks, but greater than the C task (T = P > C), and activation in the right anterior cingulate was greater for the T than the P and C tasks (T > P = C). Despite nonsignificant interactions in the left precentral gyrus and STG, planned comparisons suggested different task-related activation patterns in the 2 phases. During interval encoding, both regions exhibited greater activation for the T than the P and C tasks (T > P = C), whereas during the maintenance phase, activation was greatest for the T task and least for the C task (T > P > C).

Decision Phase

Results of the voxelwise analysis during the "decide" phase revealed multiple cortical and subcortical regions of activation related to various pairwise task comparisons (Fig. 6 and Table 3). Our main analyses focused on the fROIs derived from the decide conjunction map (Fig. 7). One-way ANOVAs performed on the decision AUC measure showed main task effects in most of the fROIs identified by the voxelwise analyses. Table 4 and Figure 8 summarize the results from these analyses. Post hoc tests revealed that most regions (i.e., anterior cingulate, bilateral middle-frontal gyrus, right IFG, bilateral insula, left IPL, pre-SMA, bilateral BG, bilateral superior cerebellum, and the pons) demonstrated a significant ($P < 0.05$) stepwise reduction in activation across the 3 tasks, such that activation was greatest for the T task and the least for the C task (T > P > C; Fig. 8). Several regions (i.e., bilateral STG, right MTG, pre-SMA/SMA, right IPL, bilateral thalamus, and left inferior cerebellum) demonstrated greater activation for the T task relative to the P and C tasks (T > P = C). One region, the left IFG, demonstrated similar activation for both the T and P tasks relative to the C task (T = P > C).

Discussion

Our results indicated that task-related striatal activation patterns during the encoding, maintenance and decision phases could be distinguished from those observed in the SMA, IFG, thalamus, frontoparietal cortices, and cerebellum. In the following sections, we discuss the roles of the striatum, the cortex, and the cerebellum in the cognitive phases involved in duration and identity processing.

Striatum

Striatal activation was greater when encoding duration than pitch but was similar when maintaining duration and pitch in WM. In the decision phase, a stepwise reduction in striatal activation was found across the 3 tasks, with the greatest activation during time perception and weakest during the sensorimotor control task. Because discrimination difficulty was well matched between the T and P tasks, our findings more

Table 3
Regions of activation from the voxelwise analysis of task effects for the decision phase

Region	T > C				P > C				T > P			
	x	*y*	*z*	Vol.	*x*	*y*	*z*	Vol.	*x*	*y*	*z*	Vol.
Frontal lobe												
[1] L inferior frontal, insula precentral (9,13,44,45)	−41	12	17	26.81	−44	19	18	7.57				
[2] R inferior frontal, middle frontal, insula (9,13,44,45)	36	17	17	21.08								
[3] B Pre-SMA/SMA, anterior cingulate (6,8,32)	0	18	41	17.34					0	11	44	4.93
[4] L anterior cingulate (32)					−6	23	41	0.78				
[5] R anterior cingulate (8,32)					9	21	39	0.38				
[6] R middle frontal (45,46)					43	26	23	1.48				
[7] L superior frontal (10)	−35	47	14	0.43								
Parietal lobe												
[8] L inferior parietal (7,40)	−38	−46	42	9.62	−33	−49	41	0.35				
[9] R inferior parietal (40)	41	−46	40	4.90					39	−43	43	0.45
[10] R SMG (40)									52	−46	34	0.44
Temporal lobe												
[11] R middle temporal (20)	55	−37	−10	0.60								
[12] L middle, superior temporal (21)	−53	−23	0	0.82								
[13] L superior temporal (13)	−53	−39	16	1.30					−42	−39	19	0.42
Limbic system												
[14] L insula (44)									−45	7	10	0.49
[15] L thalamus	−12	−13	8	0.39								
[16] R Thalamus	7	−16	4	0.50								
Basal ganglia												
[17] R caudate					11	6	3	1.17				
[18] R globus pallidus, caudate	12	3	4	0.59								
[19] L globus pallidus, putamen, caudate	−14	9	−1	1.23								
Cerebellum												
[20] B lobules IV,V,VI	−5	−43	−23	1.99								
[21] L lobules VIIB	−11	−68	−31	1.56					−11	−68	−32	0.91
[22] B pons	1	−17	−26	0.65								
Total activation volume				**89.81**				**11.73**				**7.64**

Note: Numbers on the left in brackets refer to brain regions displayed in Figure 6. Numbers in parentheses after the region label refer to Brodmann areas defined by the Talairach and Tournoux (1988) atlas. Cerebellar lobules were defined by the Schmahmann et al. (2000) atlas. There were no significant regions of activation for the C > T, C > P, or P > T comparisons. Coordinates represent distance in mm from anterior commissure: *x*, right (+)/left (−); *y*, anterior (+)/posterior (−); *z*, superior (+)/inferior (−). Vol. = volume; L = left; R = right; B = bilateral; and SMG = supramarginal gyrus.

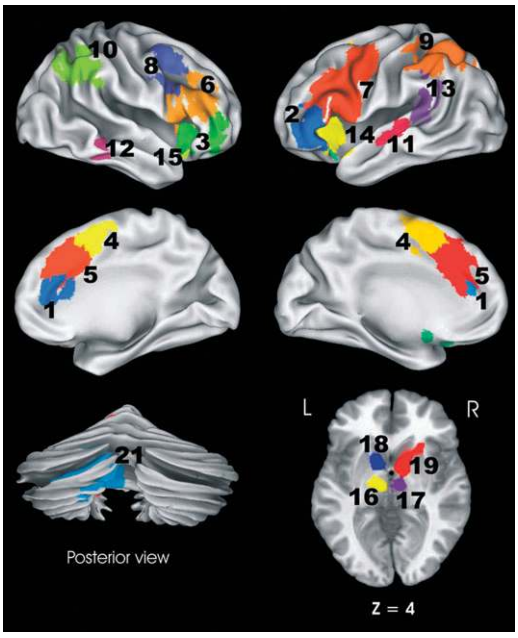

Figure 7. Functional ROIs for the decision phase used to evaluate differences in MR signal intensity across the T, P, and C tasks. Numbers adjacent to activation foci correspond to numbers in Table 4.

likely reflect differences in striatal engagement for the purpose of timing than for detection of a relevant event. Altogether, changes in striatal activation across the different phases is in keeping with its hypothesized role in detecting synchronized cortical oscillations that represent identity and temporal information (Matell and Meck 2004; Hazy et al. 2006).

Though the striatum's role in encoding has not been widely studied, coincidence detection by the striatum should enable gating of different types of information into WM (McNab and Klingberg 2008), as the present study found for the encoding of time, pitch, and basic sensory information. In the SBF model, a context-specific "time stamp" can also be built for identity information with experience. This process may begin with a phasic dopamine pulse signaling the onset of relevant stimuli and leading to synchronous firing of cortical neuronal ensembles. Cortical activity serves as the onset of the clock signal and striatal neurons are integrators of these signals. At stimulus offset, another phasic dopamine pulse strengthens corticostriatal connections, thereby gradually developing a coincidence detector for specific signal durations. Thus, the striatum functions as a core timer by integrating oscillatory states throughout a stimulus event (Matell and Meck 2004). Support for this model comes from animal studies showing that firing of striatal neurons peaks at the time of target durations, irrespective of motor output (Matell et al. 2003). In humans, the substantia nigra pars compacta exhibits time-specific activation (Jahanshahi et al. 2006). Likewise, striatal activation increases with stimulus duration (Pouthas et al. 2005) and speed-based time estimation (Beudel et al. 2009), and correlates with timing efficiency during interval encoding (Harrington et al. 2004). Our results further suggest that striatal

Table 4

Functional ROIs and summary of task effects for the decision phase

Region	*x*	*y*	*z*	Volume	*P*	η^2	Contrast
Frontal lobe							
[1] B anterior cingulate	8	30	20	1.43	0.0001	0.42	T > P > C
[2] L inferior frontal (45)	−45	32	4	3.70	0.0001	0.53	T = P > C
[3] R inferior, middle frontal (10)	38	39	1	2.22	0.0001	0.55	T > P > C
[4] B pre-SMA/SMA, anterior cingulate (6)	−4	5	53	4.86	0.0001	0.50	T > P = C
[5] B pre-SMA, anterior cingulate (6,8,32)	1	21	39	11.93	0.0001	0.54	T > P > C
[6] R middle, inferior frontal (45,46)	44	19	21	9.43	0.0001	0.53	T > P > C
[7] L middle, inferior frontal, precentral (9,44,45)	−44	9	25	17.37	0.0001	0.60	T > P > C
[8] R middle, inferior frontal, precentral gyrus (44)	41	5	39	3.15	0.0001	0.43	T > P > C
Parietal lobe							
[9] L inferior parietal (40)	−38	−46	42	9.62	0.0001	0.51	T > P > C
[10] R inferior parietal, SMG (40)	42	−46	40	5.24	0.0001	0.48	T > P = C
Temporal lobe							
[11] L superior temporal (21)	−54	−23	0	0.68	0.001	0.36	T > P = C
[12] R middle temporal (20)	54	−37	−10	0.45	0.001	0.36	T > P = C
[13] L superior temporal (13)	−51	−40	16	1.51	0.001	0.38	T > P = C
Limbic system							
[14] L insula (13)	−35	16	2	4.08	0.0001	0.52	T > P > C
[15] R insula (13)	36	20	0	2.01	0.0001	0.47	T > P > C
[16] L thalamus	−12	−14	8	1.78	0.01	0.28	T > P = C
[17] R thalamus	8	−16	6	1.92	0.001	0.31	T > P = C
Basal ganglia							
[18] L putamen, caudate	−14	7	1	3.47	0.0001	0.43	T > P > C
[19] R putamen, caudate, globus pallidus	14	7	3	5.88	0.0001	0.49	T > P > C
Cerebellum							
[20] B lobules IV, V, VI	−5	−43	−23	1.99	0.0001	0.48	T > P > C
[21] L lobules VIIB	−12	−69	−31	1.52	0.0001	0.58	T > P = C
[22] B pons	1	−17	−26	0.65	0.0001	0.47	T > P > C

Note: Numbers on the left refer to brain regions displayed in Figure 7. Numbers in parentheses after the region label refer to Brodmann areas defined by the Talairach and Tournoux (1988) atlas. Cerebellar lobules were defined by the Schmahmann et al. (2000) atlas. Coordinates represent distance in mm from anterior commissure: *x*, right (+)/left (−); *y*, anterior (+)/posterior (−); *z*, superior (+)/inferior (−). *P* values are the result of the repeated-measures ANOVA. L = left; R = right; B = bilateral; and SMG = supramarginal gyrus.

resources are utilized more when oscillatory states are integrated over time than when identity (i.e., pitch) can be ascertained from a pattern of cortical neuronal ensembles (Bendor and Wang 2005). Encoding the time of a visual signal also elicits greater striatal activation than encoding its hue, even when filled intervals are used (Coull et al. 2008). An intriguing possibility is that the conjunction of time and identity information might place even greater demands on striatal processing, although this has not been studied.

For the first time, we demonstrated that the striatum's role in maintaining information in WM is distinct from its role in encoding. These results contrast with previous studies (for a review, see Meck et al. 2008) wherein striatal activation in a variety of timing conditions cannot be distinguished from WM demands of tasks (e.g., Rao et al. 2001; Coull et al. 2004, 2008; Harrington et al. 2004; Pouthas et al. 2005). In our study, only during maintenance were similar levels of striatal activation found for duration and pitch. Passive maintenance of WM is thought to be controlled by recurrent excitation of PFC and sensory neurons (Hazy et al. 2006). To actively maintain information for longer periods, recurrent thalamocortical activity is required. The striatum may turn active maintenance states on and off via inhibitory action of the globus pallidus, which disinhibits the thalamus and allows recurrent thalamocortical firing. Consistent with our findings, this model would not predict a difference in striatal activity for maintaining duration or identity information, assuming equivalent WM loads. Likewise, when WM demands are low, active maintenance is not needed, consistent with low striatal activation in the control task. Alternatively, the maintenance period might engage timing because of expectancies about the length of the delay periods; if this were the case, similar levels of striatal activation would be expected in the control task, which was not found.

During decision making, striatal activation was robust and activated the most for time discriminations and the least in the sensorimotor control task (T > P > C). This contrasts with a report of time-related striatal activation during encoding but not decision making (Coull et al. 2008); their findings are difficult to interpret due to the absence of a sensorimotor control condition and problems with using fMRI to distinguish encoding and decision phases spaced too closely in time (1–4 s). Our results showing a stepwise pattern of striatal activation during decisional processing may be related to 2 factors. First, T > P activation may result because duration, but not identity information, becomes increasingly noisy over time due to variability of individual oscillators, which causes neuronal ensembles to loose coherence (Matell and Meck 2004) and renders decisions more difficult about the duration of a signal than its pitch. Although we did not find differences in time and pitch discrimination accuracy, difficulty in discerning temporal information may be reflected by greater utilization of cortical resources. Second, P > C activation may occur because of the striatum's role in updating WM via inhibitory and disinhibitory signals to the PFC (Hazy et al. 2006). Specifically, the globus pallidus is central for gating task-relevant information into WM (McNab and Klingberg 2008). Additionally, the caudate nuclei are engaged when manipulating information in WM (Lewis et al. 2004). Weak striatal activation in our control task likely reflects the absence of these processes.

Cortical Systems

Striatal flexibility across the different phases was accompanied by task-related activation in interconnecting cortical regions: pre-SMA/SMA, anterior cingulate, middle frontal, inferior parietal, and lateral temporal. A functional connectivity analysis identified

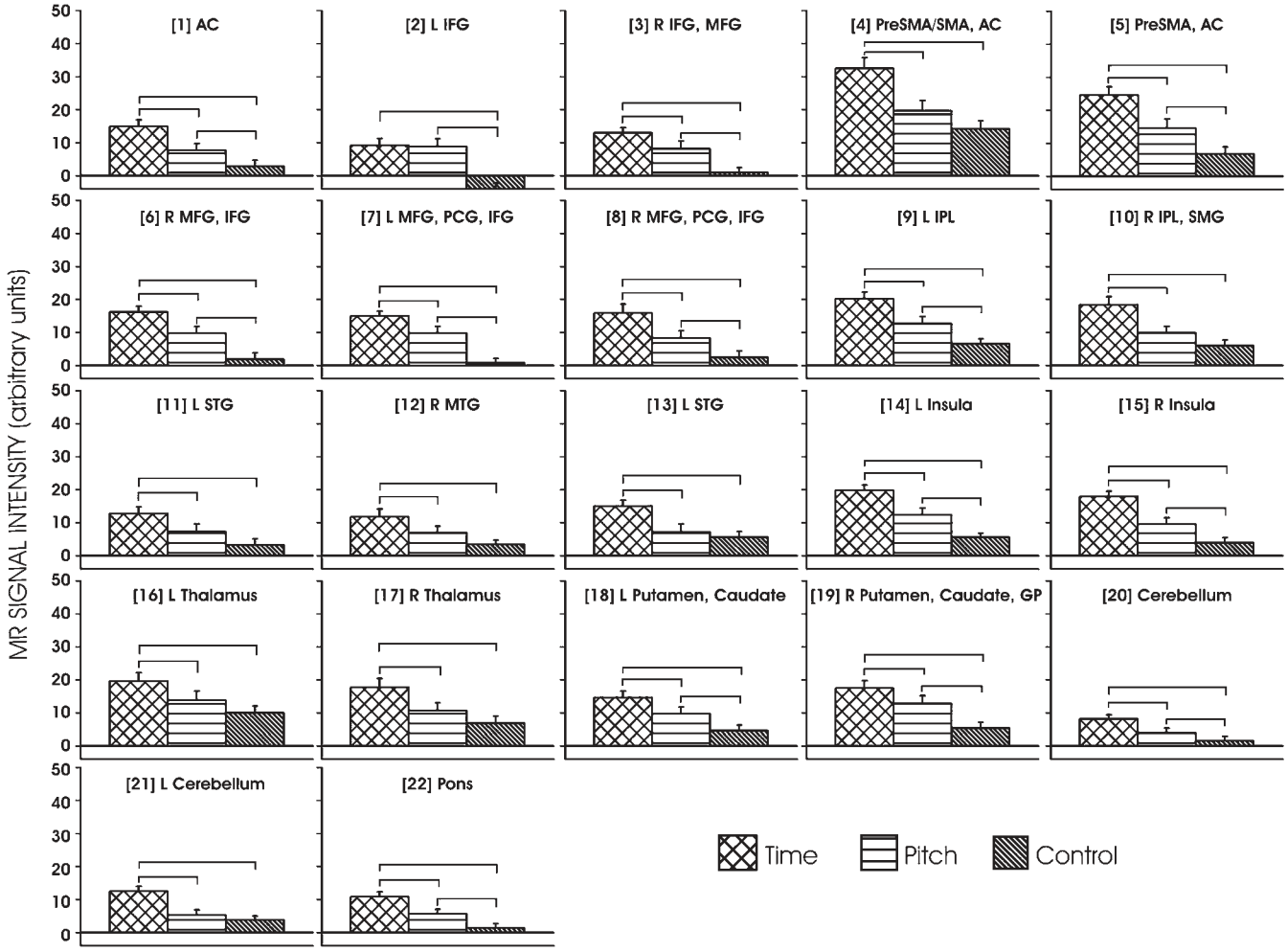

Figure 8. MR signal intensity for the T, P, and C tasks within each decision phase functional ROI. Bracketed numbers refer to brain regions listed in Table 4 and displayed in Figure 7; Horizontal lines indicate significant ($P < 0.05$) differences between conditions based on post hoc testing; error bars = SEM. R = right; L = left; AC = anterior cingulate; MFG = middle-frontal gyrus; PCG = precentral gyrus; IPL = inferior-parietal lobule; SMG = supramarginal gyrus; STG = superior temporal gyrus; MTG = middle temporal gyrus; and GP = globus pallidus.

these regions as comprising a network associated with timing movements (Stevens et al. 2007). We found that interval encoding, which provides the purest window into timekeeping networks, was related to a subset of these regions (striatum, insula, pre-SMA/SMA, cingulate, and temporal cortex). These regions and others (pre and postcentral gyrus, inferior frontal) also exhibited task-related activation during the maintenance and decision phases. In contrast, the thalamus, middle-frontal cortex, and inferior-parietal cortex showed task-related activation only during the decision phase, thereby implicating them in executive or integrative processing. These activation patterns have implications for the function of corticostriatal networks in temporal and nontemporal processing.

The striatum and areas comprising the motor circuit (pre-SMA/SMA, precentral gyrus) exhibited greater activation when encoding time than pitch or basic sensory features (T > P = C). Both the pre-SMA and SMA have dense projections to the striatum (Inase et al. 1999), which is the predominant source of input to these areas via the thalamus (Akkal et al. 2007). The pre-SMA/SMA is thought to play a key role in temporal processing (Ferrandez et al. 2003; Macar et al. 2004; Coull et al. 2008); like the basal ganglia, activation increases with target duration (Pouthas et al. 2005). However, many regions (e.g., premotor cortex, insula, inferior frontal cortex, and parietal cortex) exhibit duration-related activation (Leon and Shadlen 2003; Pouthas et al. 2005; Genovesio et al. 2006), such that this does not distinguish pre-SMA/SMA function. In our study, the key distinction between the striatum and the SMA was the task-related activation pattern during the maintenance phase. Maintenance by not only the pre-SMA/SMA but also the precentral gyrus and sensory areas was more demanding for duration than pitch (Table 2 and Fig. 5), despite no differences in task performance. This is consistent with greater pre-SMA activation in a difficult control task (color discrimination) than in an interval discrimination task, which contrasted with the opposite activation pattern in the basal ganglia (Livesey et al. 2007). Together with similar reports (Nenadic et al. 2003), it appears that the pre-SMA/SMA is not specifically concerned with interval timing. In other behavioral contexts, the SMA and premotor cortex, but not the striatum, are influenced by task complexity during movement (Elsinger et al. 2006), consistent with their role in storage or retrieval of representations (Chen et al. 1995; Lemus et al. 2007; Nakajima et al. 2009).

Task-related activation of the articulatory circuit (superior temporal, IFG, insula) was similar to the striatum during interval encoding, except in the IFG (T = P > C). The IFG inhibits prepotent responses, presumably by excitation of the subthalamic nucleus via the hyperdirect pathway, which then excites the pallidum and inhibits thalamocortical output (Aron, Durston, et al. 2007). Fiber pathways between IFG and pre-SMA (Aron, Behrens, et al. 2007) may be a route by which the IFG stops accumulation of sensory information into SMA at the offset of standard and comparison signals. This prospect is compatible with the same maintenance-period activation pattern of the insula, which also inhibits speech (Xue et al. 2008). Unlike the IFG, the insula exhibits the greatest activation during temporal encoding and decision making, presumably due to the greater integration demands of duration than pitch processing.

In the middle-frontal and inferior-parietal cortices, task-related activation did not emerge until the decision phase and was weakest in the control task. Activity in this network correlates with time-discrimination difficulty (Harrington et al. 2004), consistent with its modulation of executive functions. Greater activity for time than pitch discriminations, despite similar levels of accuracy, suggests that utilization of neuronal resources may be a more sensitive indicator of executive demands than behavior. Hemispheric differences were also noted, wherein P > C activation was found for left, but not right, inferior-parietal cortex. Left hemisphere damage produces deficits in both time and pitch discriminations, whereas right inferior-parietal cortex lesions specifically disrupt time perception (Harrington et al. 1998). One speculation is that these hemispheric differences may reflect engagement of right parietal resources for temporal integration and left parietal mechanisms for discerning magnitude (Hubbard et al. 2005).

Cerebellum

The striatum and cerebellum were also distinguished by their activation patterns. Unlike the striatum, task-related cerebellar activation did not occur during encoding or maintenance, inconsistent with its role as a core timekeeper (Ivry et al. 2002). A recent study of patients with cerebellar damage suggests that the cerebellum supports discrete and continuous forms of timing possibly by acting as a forward model, predicting and adapting behavioral states based on efferent copy of sensory and motor information (Bo et al. 2008). This mechanism may fine tune and adjust sensory states during temporal and nontemporal decision making, perhaps by aiding in the detection of mismatches between predicted and current sensory signals (Blakemore et al. 1999). Connectivity with the pre-SMA/SMA (Akkal et al. 2007) may provide the anatomical means by which stored sensory representations are accessed and utilized by the cerebellum.

Summary

In conclusion, by separating activation associated with different trial components, our findings are consistent with a hybrid model (Lustig et al. 2005), which posits that timing emerges from context-dependent interactions among corticostriatal circuits. This is a powerful framework as it provides a mechanism by which the striatum modulates temporal and nontemporal processing.

Funding

National Institutes of Health (P01 MH51358, M01 RR00058); the Department of Veterans Affairs.

Notes

We would like to thank Sally Durgerian for her technical support.
Conflict of Interest: None declared.

Address correspondence to email: RAOS2@ccf.org.

References

Akkal D, Dum RP, Strick PL. 2007. Supplementary motor area and presupplementary motor area: targets of basal ganglia and cerebellar output. J Neurosci. 27:10659–10673.

Aron AR, Behrens TE, Smith S, Frank MJ, Poldrack RA. 2007. Triangulating a cognitive control network using diffusion-weighted magnetic resonance imaging (MRI) and functional MRI. J Neurosci. 27:3743–3752.

Aron AR, Durston S, Eagle DM, Logan GD, Stinear CM, Stuphorn V. 2007. Converging evidence for a fronto-basal-ganglia network for inhibitory control of action and cognition. J Neurosci. 27:11860–11864.

Bendor D, Wang X. 2005. The neuronal representation of pitch in primate auditory cortex. Nature. 436:1161–1165.

Beudel M, Renken R, Leenders KL, de Jong BM. 2009. Cerebral representations of space and time. Neuroimage. 44:1032–1040.

Blakemore SJ, Wolpert DM, Frith CD. 1999. The cerebellum contributes to somatosensory cortical activity during self-produced tactile stimulation. Neuroimage. 10:448–459.

Bo J, Block HJ, Clark JE, Bastian AJ. 2008. A cerebellar deficit in sensorimotor prediction explains movement timing variability. J Neurophysiol. 100:2825–2832.

Chen Y-C, Thaler D, Nixon PD, Stern C, Passingham RE. 1995. The functions of the medial premotor cortex (SMA) II. The timing and selection of learned movements. Exp Aging Res. 102:461–473.

Coull JT, Nazarian B, Vidal F. 2008. Timing, storage, and comparison of stimulus duration engage discrete anatomical components of a perceptual timing network. J Cogn Neurosci. 20:2185–2197.

Coull JT, Vidal F, Nazarian B, Macar F. 2004. Functional anatomy of the attentional modulation of time estimation. Science. 303:1506–1508.

Cox RW. 1996. AFNI: software for analysis and visualization of functional magnetic resonance neuroimages. Compar Biomed Res. 29:162–173.

Elsinger CL, Harrington DL, Rao SM. 2006. From preparation to online control: reappraisal of neural circuitry mediating internally generated and externally guided actions. Neuroimage. 31:1177–1187.

Ferrandez AM, Hugueville L, Lehericy S, Poline JB, Marsault C, Pouthas V. 2003. Basal ganglia and supplementary motor area subtend duration perception: an fMRI study. Neuroimage. 19:1532–1544.

Genovesio A, Tsujimoto S, Wise SP. 2006. Neuronal activity related to elapsed time in prefrontal cortex. J Neurophysiol. 95:3281–3285.

Gibbon J, Church RM, Meck WH. 1984. Scalar timing in memory. Ann NY Acad Sci. 423:52–77.

Harrington DL, Boyd LA, Mayer AR, Sheltraw DM, Lee RR, Huang M, Rao SM. 2004. Neural representation of interval encoding and decision making. Cogn Brain Res. 21:193–205.

Harrington DL, Haaland KY, Knight RT. 1998. Cortical networks underlying mechanisms of time perception. J Neurosci. 18:1085–1095.

Hazy TE, Frank MJ, O'Reilly RC. 2006. Banishing the homunculus: making working memory work. Neuroscience. 139:105–118.

Hubbard EM, Piazza M, Pinel P, Dehaene S. 2005. Interactions between number and space in parietal cortex. Nat Rev Neurosci. 6: 435–448.

Inase M, Tokuno H, Nambu A, Akazawa T, Takada M. 1999. Corticostriatal and corticosubthalamic input zones from the presupplementary motor area in the macaque monkey: comparison with the input zones from the supplementary motor area. Brain Res. 833:191–201.

Ivry RB, Spencer RM, Zelaznik HN, Diedrichsen J. 2002. The cerebellum and event timing. Ann N Y Acad Sci. 978:302–317.

Jahanshahi M, Jones CR, Dirnberger G, Frith CD. 2006. The substantia nigra pars compacta and temporal processing. J Neurosci. 26:12266–12273.
Lemus L, Hernandez A, Luna R, Zainos A, Nacher V, Romo R. 2007. Neural correlates of a postponed decision report. Proc Natl Acad Sci USA. 104:17174–17179.
Leon MI, Shadlen MN. 2003. Representation of time by neurons in the posterior parietal cortex of the macaque. Neuron. 38:317–327.
Lewis SJ, Dove A, Robbins TW, Barker RA, Owen AM. 2004. Striatal contributions to working memory: a functional magnetic resonance imaging study in humans. Eur J Neurosci. 19:755–760.
Livesey AC, Wall MB, Smith AT. 2007. Time perception: manipulation of task difficulty dissociates clock functions from other cognitive demands. Neuropsychologia. 45:321–331.
Lustig C, Matell MS, Meck WH. 2005. Not "just" a coincidence: frontal-striatal interactions in working memory and interval timing. Memory. 13:441–448.
Macar F, Anton JL, Bonnet M, Vidal F. 2004. Timing functions of the supplementary motor area: an event-related fMRI study. Cogn Brain Res. 21:206–215.
Matell MS, Meck WH. 2004. Cortico-striatal circuits and interval timing: coincidence detection of oscillatory processes. Cogn Brain Res. 21:139–170.
Matell MS, Meck WH, Nicolelis MA. 2003. Interval timing and the encoding of signal duration by ensembles of cortical and striatal neurons. Behav Neurosci. 117:760–773.
McNab F, Klingberg T. 2008. Prefrontal cortex and basal ganglia control access to working memory. Nat Neurosci. 11:103–107.
Meck WH. 1983. Selective adjustment of the speed of internal clock and memory processes. J Exp Psychol Anim Beh Proc. 9:171–201.
Meck WH. 1996. Neuropharmacology of timing and time perception. Cogn Brain Res. 3:227–242.
Meck WH, Penney TB, Pouthas V. 2008. Cortico-striatal representation of time in animals and humans. Curr Opin Neurobiol. 18:145–152.
Nakajima T, Hosaka R, Mushiake H, Tanji J. 2009. Covert representation of second-next movement in the pre-supplementary motor area of monkeys. J Neurophysiol. 101:1883–1889.
Nenadic I, Gaser C, Volz HP, Rammsayer T, Hager F, Sauer H. 2003. Processing of temporal information and the basal ganglia: new evidence from fMRI. Exp Brain Res. 148:238–246.
Oldfield RC. 1971. The assessment and analysis of handedness: The Edinburgh Inventory. Neuropsychologia. 9:97–113.
Postle BR, D'Esposito M. 1999. Dissociation of human caudate nucleus activity in spatial and nonspatial working memory: an event-related fMRI study. Cogn Brain Res. 8:107–115.
Pouthas V, George N, Poline JB, Pfeuty M, Vandemoorteele PF, Hugueville L, Ferrandez AM, Lehericy S, LeBihan D, Renault B. 2005. Neural network involved in time perception: an fMRI study comparing long and short interval estimation. Hum Brain Mapp. 25:433–441.
Rao SM, Mayer AR, Harrington DL. 2001. The evolution of brain activation during temporal processing. Nat Neurosci. 4:317–323.
Schmahmann J, Doyon J, Toga A, Petrides M, Evans A. 2000. MRI Atlas of the Human Cerebellum. San Diego: Academic Press.
Stevens MC, Kiehl KA, Pearlson G, Calhoun VD. 2007. Functional neural circuits for mental timekeeping. Hum Brain Mapp. 28:394–408.
Talairach J, Tournoux P. 1988. Co-planar stereotaxic atlas of the human brain. New York: Thieme.
Worsley KJ, Marrett S, Neelin P, Vandal AC, Friston KJ, Evans AC. 1996. A unified statistical approach for determining significant signals in images of cerebral activation. Hum Brain Mapp. 4:58–73.
Xue G, Aron AR, Poldrack RA. 2008. Common neural substrates for inhibition of spoken and manual responses. Cereb Cortex. 18:1923–1932.